Architecture dependence of photon antibunching in cavity quantum electrodynamics

Matthew Bradford and Jung-Tsung Shen*

Department of Electrical and Systems Engineering, Washington University in St. Louis, St. Louis, Missouri 63130, USA

(Received 27 August 2014; published 10 August 2015)

We investigate numerically the architecture dependence of the characteristics of antibunched photons generated in cavity quantum electrodynamic systems. We show that the quality of antibunching [the smallness of the second-order intensity correlation function at zero time $g^{(2)}(0)$] and the generation efficiency significantly depend on the configurations: the arrangements of single-mode optical cavities and waveguides. We found that for certain class of architecture, when the Jaynes-Cummings system (the atom-cavity system) couples to two terminated waveguides, there exists a fundamental tradeoff between high transmission and low $g^{(2)}(0)$, and is sensitive to dissipation. We further show that optimal antibunching can be achieved in two alternative cavity quantum electrodynamic configurations operating in the dissipatively weak coupling regime such that the two-photon transmission can be two orders of magnitude higher for the same $g^{(2)}(0)$.

DOI: 10.1103/PhysRevA.92.023810 PACS number(s): 42.50.Pq, 42.50.Ar, 03.65.Nk, 72.10.Fk

I. INTRODUCTION

Photon antibunching refers to the statistical property of a light field that the probability to detect two photons right after each other vanishes [1–5]. Photon antibunching demonstrates the manifestly quantum character of light, as a classical theory of fluctuating field amplitudes would require negative probability in order to give antibunching. Photon bunching describes the opposite effect that the probability to detect a photon immediately after another one has been found is higher than at a later moment. The photon statistics of a light beam is characterized by measurement of the normalized second-order intensity correlation function $g^{(2)}(\tau)$, which characterizes the joint probability of detecting one photon followed by another within the delay time τ. For perfectly antibunched light beam, the intensity correlations vanish for short delay times. In practice, often a less stringent criterion for antibunching is used: the initial slope of $g^{(2)}(\tau)$ is positive [i.e., $g^{(2)}(0) < g^{(2)}(\tau)$], which means the probability for coincidence ($\tau = 0$) is smaller than noncoincidence ($\tau \neq 0$). Under the latter criterion, the photon-counting statistics of antibunched photons can be either super-Poissonian [$g^{(2)}(0) > 1$] or sub-Poissonian [$g^{(2)}(0) < 1$] [6,7]. A stream of photons that is both antibunched and sub-Poissonian has a subshot noise power level that is below the standard quantum limit and can serve as single-photon light sources [8–10]; such light sources are important for applications in quantum information science, including absolutely secure quantum communication [11], single-photon interferometry [12] and interaction-free measurement [13], and quantum computation with linear optics [14].

It was first theoretically predicted that the resonance fluorescence of a two-level atom driven by a resonant laser field would exhibit photon antibunching [15,16], and subsequently in 1977 Kimble, Dagenais, and Mandel observed the phenomenon of antibunching by using sodium atoms in an atomic beam [17]. In 1997, Höffges *et al.* observed photonic antibunching from the spectrum of the fluorescent radiation of a single quantum emitter (a trapped $^{24}Mg^{+}$ ion) [18]. In recent years, stemming from the applications in quantum information processing and also from the rapidly advanced experimental techniques, there has been greatly growing interest in generating such nonclassical photonic states in various cavity quantum electrodynamics (QED) systems containing only one single quantum emitter [19–26]. To quantify the characteristics of antibunched photons generated in cavity QED, the first important metrics is the *quality of antibunching*, i.e., the smallness of $g^{(2)}(0)$ which measures the overlap between photons. Ideal single-photon sources would have $g^{(2)}(0) = 0$. The issue of quality of antibunching in cavity QED has been recognized and discussed extensively in the literatures using a master-equation approach [27–32]. The second important metrics concerns the *generation efficiency* of the antibunched photons. For a continuous coherent driving field, the generation efficiency can be properly defined as the ratio of flux of the generated antibunched photons to the flux of the driving optical field. Another scenario of interest is the generation of antibunched photons from a Fock state input containing a fixed number of uncorrelated photons. For example, for a pulse containing two uncorrelated photons, the generation efficiency is the probability the two photons become antibunched after scattering. In the weak coherent driving regime, these two descriptions are asymptotically equivalent. The issue of generation efficiency so far has received less attention in the context of cavity QED (we note that large antibunching and high generation efficiency have been discussed and demonstrated in the context of Rydberg polaritons [33,34]). In cavity QED, even if the configuration is set up so that individual photons have perfect transmission, and that the antibunched photons are generated in the transmitted direction, in general, a significant portion of incoming photons in a multiphoton state (coherent or Fock state) can still be reflected due to correlations.

More importantly, the cavity QED systems, in particular in the solid-state implementations, allow us to explore a wide variety of structural couplings between the photonic modes via different arrangements of optical resonators and waveguides. Such a possibility suggests the need for an investigation of the impacts of the structural configurations of optical components on the characteristics, the quality and the generation efficiency, of antibunched photons created in cavity QED.

This paper is devoted to investigating numerically the architecture dependence of photon antibunching in cavity QED.

*jushen@wustl.edu

Specifically, we will discuss the characteristics of antibunched photons in three different configurations in cavity QED, involving different arrangements of optical cavities and waveguides. For brevity, we shall call each configuration a cQED circuit. This paper will focus on resonators of single-mode cavities; the cases of optimal antibunching in configurations involving whispering-gallery-type optical resonators [35,36], which have degenerated counterpropagating modes, will be presented elsewhere. We do this by first numerically evolving the photonic states temporally in cQED circuits of different architectures, determining the statistical properties from the scattered photonic states. Then, for each architecture, we numerically scan a range of coupling strengths between the atom-cavity-waveguide system to investigate the fundamental and optimal performance of each architecture. To emphasize the structural impacts on the generation characteristics of antibunched photons, we first discuss the cases wherein the intrinsic dissipations (which take photons out of the system in question) are not present to demonstrate the fundamental limitations of each architecture; we then present the results when realistic numerical values of dissipations, taken from appropriate experimental data, are considered. Using such an approach, we first show that the cQED circuit architecture employed in many current cavity QED experiments to generate antibunched photons, wherein a Jaynes-Cummings (JC) system [37,38] couples to input and output waveguides to form an inline configuration, has an intrinsic tradeoff between high-generation efficiency and low $g^{(2)}(0)$, which remains so even for the ideal case where the dissipations are not present. We then demonstrate that for two different cQED circuits, with an architecture of either a side-coupled JC system or a direct-coupled generalized JC configuration, the generation of antibunched photons can be two orders of magnitude more efficient or the quality can be at least 10 times better, operating in the dissipatively weak coupling regime.

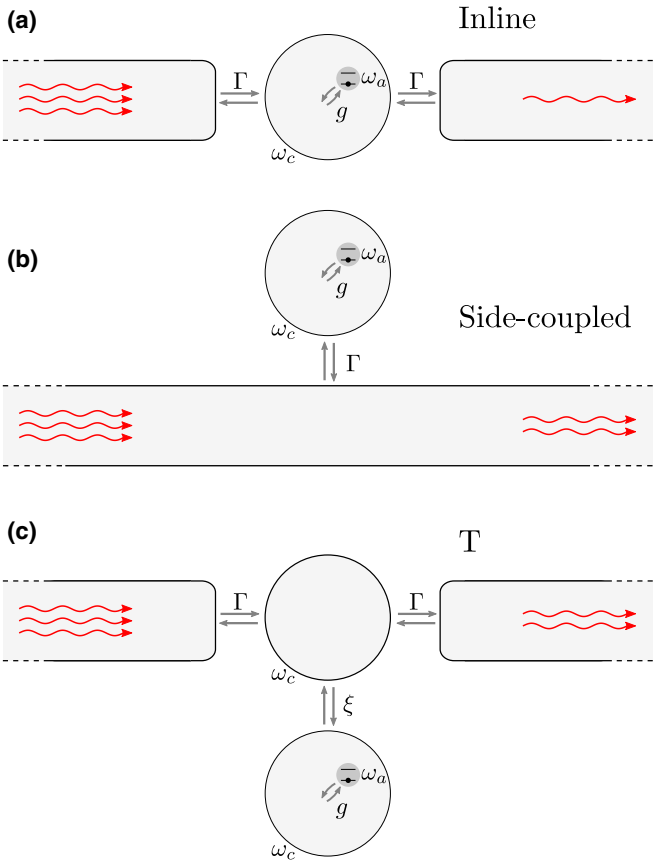

FIG. 1. (Color online) Cavity QED circuits exhibiting photon blockade for the transmission field. (a) Inline geometry with a JC system placed between two terminated waveguides. (b) Side-coupled geometry with a JC system coupled to a single waveguide. (c) T geometry with a generalized JC system coupled to two terminated waveguides. For all configurations, Γ represents the cavity-waveguide coupling strength (i.e., halfwidth of the cavity linewidth); g represents the atom-cavity coupling strength; the intercavity coupling strength for the T geometry is given by ξ. All coupling strengths have the unit of frequency. ω_a is the angular transition frequency of the two-level atom, and ω_c is the resonant frequency of the cavities. The on-resonance case (that is, $\omega_a = \omega_c$) is considered throughout. Each waveguide has a single transverse mode for each operating frequency.

II. JAYNES-CUMMINGS AND GENERALIZED JAYNES-CUMMINGS SYSTEMS

The fundamental building block to generate antibunched photons in cavity QED is the Jaynes-Cummings system, which describes the interaction of a two-level atom with the quantized modes of an optical or microwave cavity [37,38]. One configuration to couple photons in and out is to employ an inline geometry by coupling a JC system to two terminated waveguides [Fig. 1(a)]. Other possible simple configurations include the side-coupled geometry, which uses a single waveguide [Fig. 1(b)]; and the T geometry wherein two terminated waveguides couple to a generalized JC system, which is formed by introducing an additional bare cavity coupled to the waveguides [Fig. 1(c)]. All waveguides are single-polarization single-mode waveguides [39] to minimize the cross talks between different modes which degrade the performance. All cQED circuits exhibit single-photon nonlinearity, as they contain a two-level atomic component that can be saturated by a single photon under ideal conditions.

Both the JC and generalized JC systems are exactly soluble (see Appendix for details). Here, we summarize the main results. As illustrated in Fig. 2(a), the underlying mechanism of the photon blockade in the inline cQED circuit is the anharmonicity of the JC ladder of eigenstates [37,40]. Each n-photon manifold consists of two dressed states $|n^+\rangle$ and $|n^-\rangle$, with a frequency separation $2\sqrt{n}g$ (g is the atom-cavity coupling strength in frequency). Thus, when a single photon of frequency $\omega_i = \omega_c - g$, which is on resonance with the state $|1^-\rangle$ of the intermediary JC component, is injected into the input port of the inline circuit, the photon will resonantly tunnel through to the output port with a relatively high probability [see Fig. 2(a) bottom for the single-photon transmission spectrum); nonetheless, when two resonant photons at frequency ω_i are injected simultaneously, the resonant absorption of either photon will "block" the absorption of a second photon. Moreover, as the sharp energy levels of the JC component will be broadened and gain a finite width $\sim\Gamma$ when coupled to the waveguide, the inline circuit must operate in the strong coupling regime [$g > \Gamma$, such that the frequency mismatch

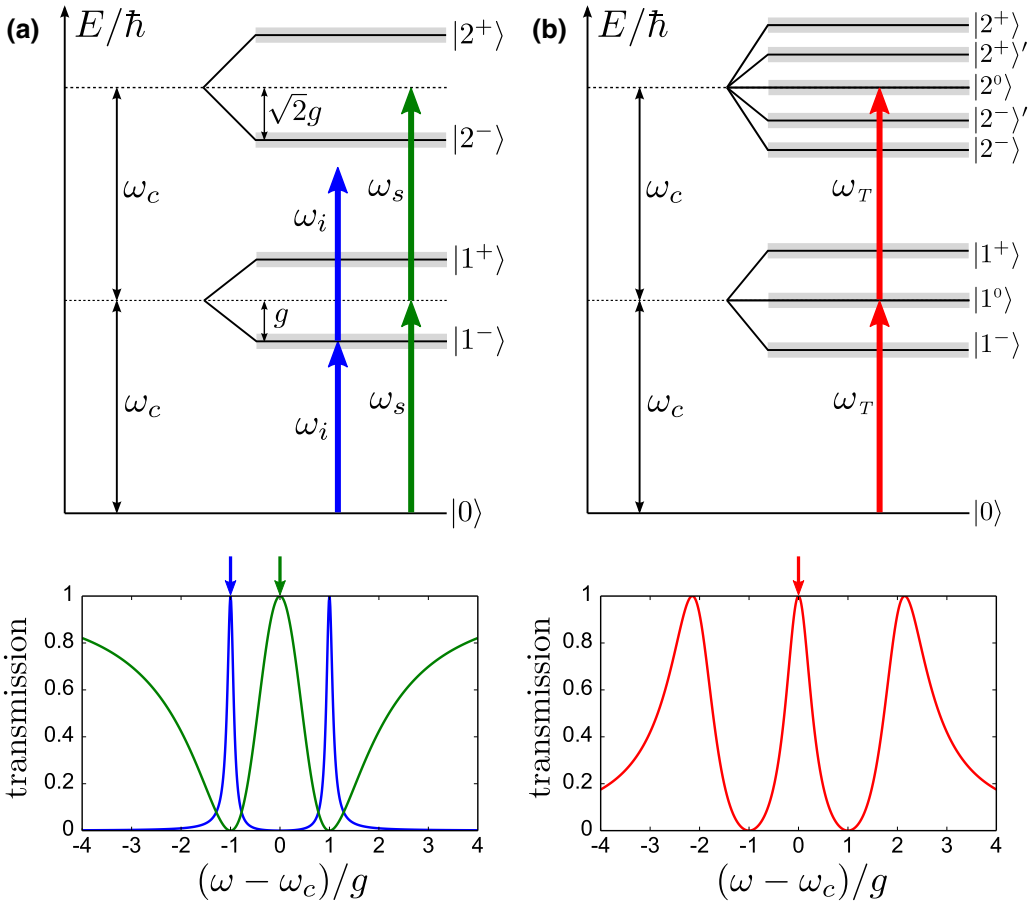

FIG. 2. (Color online) Energy-level diagrams, operating schemes, and single-photon transmission spectra for the JC and generalized JC systems. (a) Top: JC level scheme is shown up to the second manifold, with single-photon operating frequencies $\omega_i = \omega_c - g$ for the inline (blue arrows) and $\omega_s = \omega_c$ for the side-coupled (green arrows) geometries. Each n-photon manifold has two energy levels. Bottom: single-photon transmission spectrum for inline (with $\Gamma/g = 0.15$) and side-coupled (with $\Gamma/g = 1.75$) geometries with arrows indicating single-photon operating frequency [41]. (b) Top: generalized JC level scheme is shown up to the second manifold, with single-photon operating frequency $\omega_T = \omega_c$ for the T geometry (red arrows). Each n-photon manifold has $2n + 1$ energy levels. Bottom: single-photon transmission spectrum for the T geometry with $\Gamma/g = 1.4$ and $\xi/g = 1.9$. Each energy level is broadened (gray color) when coupled to the waveguide.

$(2 - \sqrt{2})g$ exceeds the finite width] so as the photon blockade mechanism to be effective.

The above picture based upon anharmonic ladder diagram and single-photon transport is often used to infer the antibunching behavior [19–23]; this noninteracting picture, however, cannot be conveniently applied to other cQED circuits, where the statistics of the transmitted photons in general are influenced by external couplings and can only be determined by the full interacting scattering dynamics that takes into account the photon-photon correlations induced by the intermediary JC interaction. For example, as will be shown later, both the side-coupled and T circuits can generate antibunched photons in the weak coupling regime, but the antibunching behavior in either configuration does not directly arise from the anharmonicity mechanism as with the inline circuit. Specifically, for the side-coupled cQED circuit with the energy level diagram and the operating scheme shown in Fig. 2(a), at the operating frequency $\omega_s = \omega_c$, high single-photon transmission is expected as the photon is not on resonance with the JC component and simply carries on unimpeded; when two photons are injected simultaneously, the full scattering dynamics indicates that the transmitted photons will be antibunched and have higher transmission efficiency than the inline case.

The energy-level diagram for the generalized JC component is shown in Fig. 2(b). Here, we summarize the relevant properties. For each n-photon manifold there are now $2n + 1$ dressed states due to the additional cavity degree of freedom. This can be deduced by exhausting all partition possibilities of the photons. For example, when $n = 1$ the three bare states are $|1,0,\text{ground}\rangle$, $|0,1,\text{ground}\rangle$, and $|0,0,\text{excited}\rangle$ where the first, second, and third slots of the state correspond to the number of photons in the bare cavity, the number of photons in the JC cavity, and the atomic state (ground or excited), respectively; the dressed states are linear combinations of the bare states. For each manifold there is always an unperturbed central energy level; the energy separations (in units of g) from the central state are functions of ξ/g. For the limiting case of large ξ/g, all dressed states are cavitylike and equally spaced in frequency. When ξ/g becomes small, the bare cavity decouples, and the eigenstates of the generalized JC component reduce to product states of the bare cavity state and the JC dressed

state: $|\text{bare cav}\rangle \otimes |\text{JC}\rangle$. The eigenstate naming convention in Fig. 2(b) is chosen to make this reduction transparent: the $|2^{\pm}\rangle$ generalized JC states reduce to $|0\rangle_{\text{cav}}|2^{\pm}\rangle_{\text{JC}}$ (i.e., both photons are in the JC component); the $|2^{\pm}\rangle'$ generalized JC states reduce to $|1\rangle_{\text{cav}}|1^{\pm}\rangle_{\text{JC}}$ (i.e., one photon is in the bare cavity, and one is in the JC component); the $|2^{0}\rangle$ generalized JC state reduces to $|2\rangle_{\text{cav}}|0\rangle_{\text{JC}}$ (i.e., both photons are in the bare cavity). For the T cQED circuit operating at frequency $\omega_T = \omega_c$ as shown in Fig. 2(b), a single resonant photon can tunnel through by interacting with the unperturbed resonance $|1^{0}\rangle$ of the generalized JC system. When two photons are injected simultaneously, the two photons will hit the unperturbed resonance of the two-photon manifold $|2^{0}\rangle$ of the generalized JC component. The full scattering dynamics indicates that the transmitted photons will also be antibunched and have a higher transmission efficiency than the inline case.

III. STATISTICAL PROPERTIES OF THE TRANSMITTED OPTICAL FIELDS

A. Input state

The statistics of the transmitted field in a cQED circuit must be determined by the interacting two-photon scattering dynamics that takes into account the photon-photon correlations induced by the intermediary JC interaction. To substantiate this interacting picture quantitatively, we inject into each circuit a two-photon input state, which is numerically evolved in time according to the equations of motion, and investigate the photon statistics for the output field by computing the normalized second-order correlation function $g^{(2)}(\tau)$ (see Appendix for details). The input state at $t = 0$ consists of two identically overlapping Gaussian wave packets with spatial width σ, center position x_0, and central frequency ω_0:

$$\phi_{\text{in}}(x_1,x_2,0) = \frac{1}{\sqrt{2\pi\sigma^2}} e^{-(x_1-x_0)^2/4\sigma^2-(x_2-x_0)^2/4\sigma^2} \times e^{i(\omega_0/v)x_1+i(\omega_0/v)x_2}, \quad (1)$$

where x_1 and x_2 correspond to the location of each photon in the input port of the waveguide, and v is the group velocity of photons in the waveguide. Such an input is a product state, meaning that the two photons are completely uncorrelated. The square amplitude $|\phi_{\text{in}}|^2$ is the probability density and is normalized to unity when integrated from $-\infty$ to ∞ in both x_1 and x_2. It can be shown both numerically and analytically that $g^{(2)}_{\text{input}}(\tau) = \frac{1}{2}$ for all τ, which is expected for a number (Fock) state [3,5]. In principle, to properly simulate a weak coherent input to obtain the photon statistics, one should use a truncated coherent input that contains the vacuum state, a one-photon state, and a two-photon state. However, either choice (a two-photon number state or a truncated coherent state) yields the same $g^{(2)}(\tau)$ (see Appendix for all technical details).

B. Scattered photon states

After scattering, there are four possible outcomes for the two photons: both transmitted, with a wave function $\phi_{RR}(x_1,x_2,t)$; both reflected, with a wave function $\phi_{LL}(x_1,x_2,t)$; as well as one transmitted and one reflected, with a wave function $\phi_{RL}(x_1,x_2,t)$ and $\phi_{LR}(x_1,x_2,t)$, respectively. Here, the subscript denotes the propagation direction of the photon after scattering: R denotes right moving, thus transmitted; and L denotes left moving, thus reflected. A graphic representation of the two-photon scattering dynamics

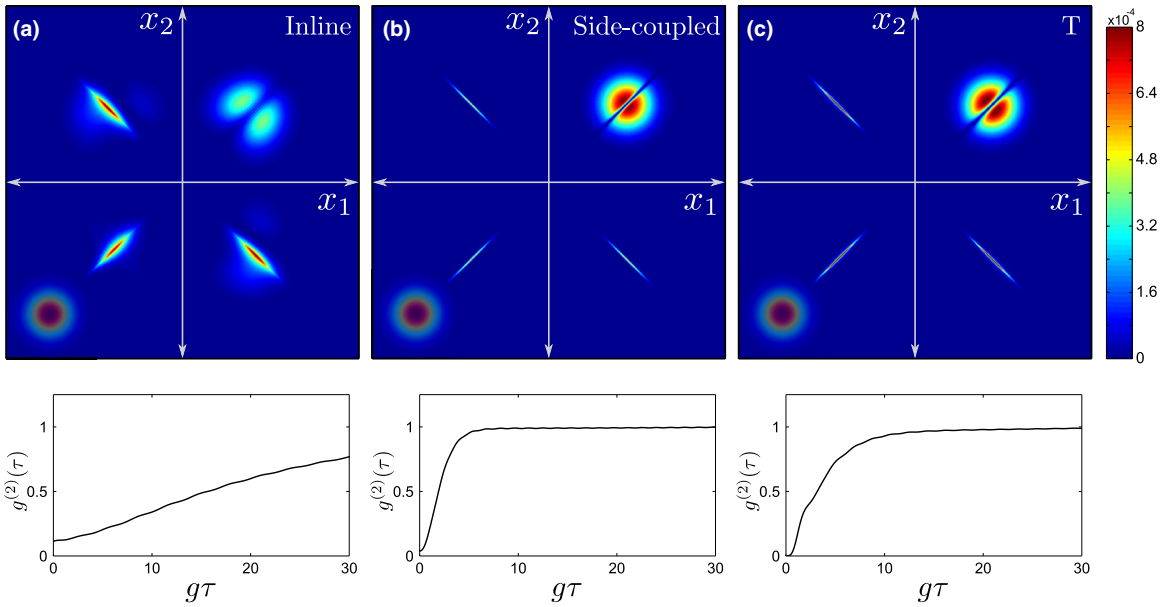

FIG. 3. (Color online) Probability density plot for two-photon transport in cQED circuits. (a) Inline geometry ($\Gamma/g = 0.15$). (b) Side-coupled geometry ($\Gamma/g = 1.75$). (c) T geometry ($\Gamma/g = 1.4$, $\xi/g = 1.9$). In each plot, the two-photon input state at $t = 0$ is shown as a disk in the third quadrant. For the output state, the part in the first quadrant corresponds to both photons transmitted; the part in the third quadrant corresponds to both photons reflected; and the parts in the second and fourth quadrants correspond to one photon transmitted and one reflected. The input state is made transparent to visually distinguish it from the output. Simulation parameters correspond to $gx_0/v = -70$, $g\sigma/v = 15$ for all cases.

for each cQED circuit is shown in Fig. 3, which plots the probability density for the input and output (long after scattering) states. In the colormap representation, the two-photon input state described by Eq. (1) will appear as a disk in the third quadrant (x_1, $x_2 < 0$). Different choices for the input will have different shapes. For the output wave function in the first quadrant $\phi_{RR}(x_1,x_2,t)$ (i.e., both photons are transmitted field), the center cut along the $x_1 = x_2$ line for each case implies photon blockade behavior, as the probability density has a depleted region corresponding to the two photons separating from each other. Conversely, in the third quadrant the output wave function $\phi_{LL}(x_1,x_2,t)$ is localized along the $x_1 = x_2$ line, exhibiting bunching behavior for the reflection field. Likewise, the localization of the wave function in the second $\phi_{LR}(x_1,x_2,t)$ and fourth quadrants $\phi_{RL}(x_1,x_2,t)$ means that the photons will be found at the same distance from the scatterer on opposite sides. By projecting the output wave function onto the relative coordinate axis ($x_1 = -x_2$ line), $g^{(2)}(\tau)$ is computed from integrating the projection along the axis (Fig. 3). The total probability for each outcome is obtained by integrating the respective probability density over each quadrant. For example, the probability of the both photons being transmitted, P_{tt}, is given by integrating $|\phi_{RR}(x_1,x_2,t)|^2$ over the first quadrant.

C. Results: Quality of antibunching and generation efficiency

While each cQED circuit exhibits sub-Poissonian and antibunching behavior [$g^{(2)}(0) \ll 1$, $g^{(2)}(0) < g^{(2)}(\tau)$], the performance differs greatly. The inline circuit has the lowest two-photon transmission probability P_{tt} and causes the most distortion in the waveform. The T geometry has the smallest $g^{(2)}(0)$, i.e., the photons are more antibunched, so to speak. Additionally, the inline geometry exhibits a much wider gap across the $x_1 = x_2$ line, so that $g^{(2)}(\tau)$ for the inline circuit rises to unity much slower than for the side-coupled and T geometries (Fig. 3); also, the center of the scattered wave function for the inline geometry lags significantly behind that of the side-coupled and T geometries. For example, for reported values of g in the optical [24] and microwave [22] regimes, the relative delay time is $\approx$0.1 or $\approx$15 ns, respectively. The delay reflects the long photon-cavity interaction time scale, which is a general feature for any system operating in the strong coupling regime. These effects fundamentally limit the operation rate of the strongly coupled cQED circuits.

Figure 4 shows the dependence of $g^{(2)}(0)$ and P_{tt} on the coupling strengths. For the inline case $g^{(2)}(0)$ falls off as Γ/g decreases, and numerically $g^{(2)}(0) \propto (\Gamma/g)^2$ for small values of Γ/g, in agreement with previous results [19]. Under this strong coupling condition, however, $P_{tt} \propto \Gamma/g$ also falls off

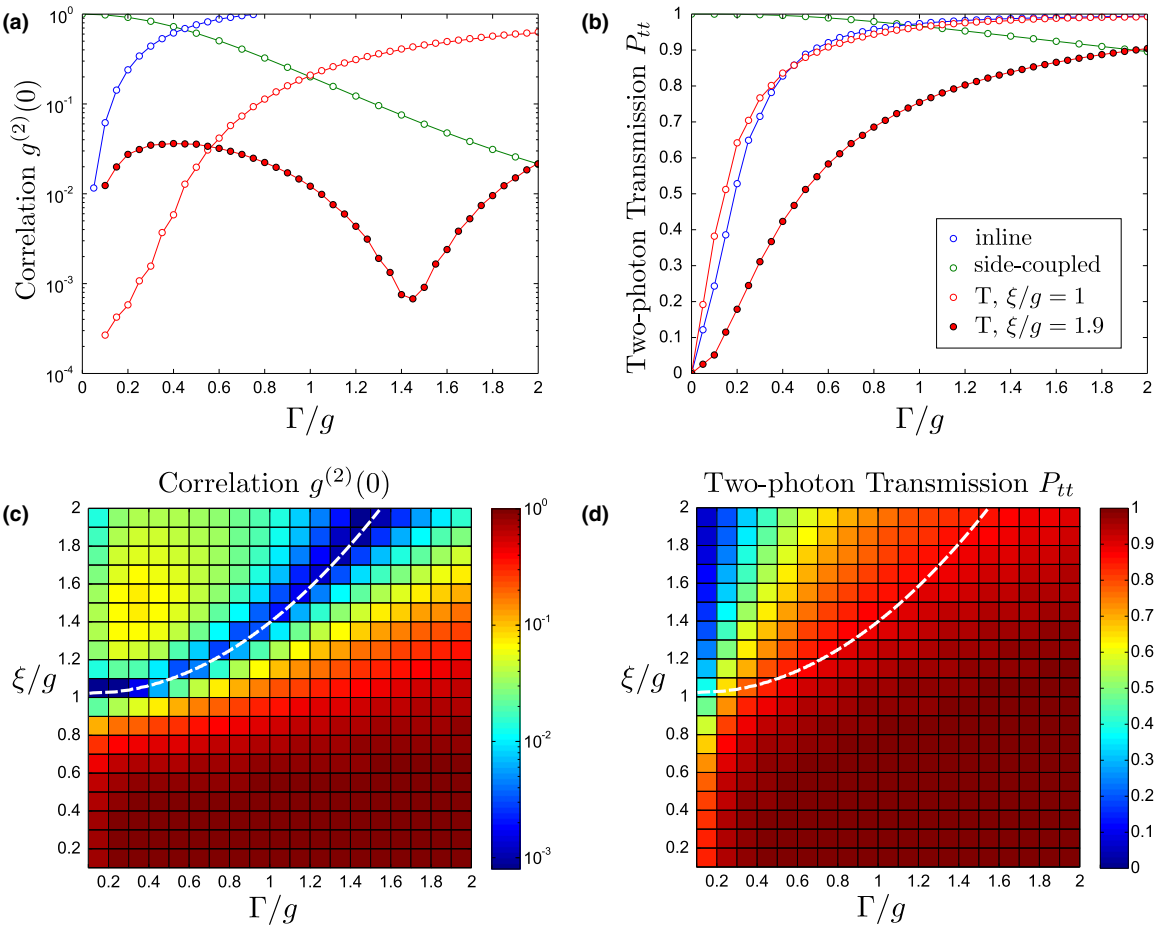

FIG. 4. (Color online) Performance plots of the cQED circuits. (a) Semilog plot of $g^{(2)}(0)$. (b) Two-photon transmission P_{tt}. (c) $g^{(2)}(0)$ versus Γ/g and ξ/g for the T geometry. (d) P_{tt} versus Γ/g and ξ/g for the T geometry. For all cases, $g\sigma/v = 15$. The white dashed line in (c) and (d) denotes the valley relation.

as Γ/g decreases. For example, to achieve $g^{(2)}(0) \approx 10^{-2}$ in the inline geometry, the strong coupling requirement leads to a $P_{tt} \approx 0.1$. In contrast, for the side-coupled case $g^{(2)}(0)$ falls off as Γ/g increases, and numerically $g^{(2)}(0) \propto e^{-2\Gamma/g}$ for $\Gamma/g \gtrsim 1$. Thus, the side-coupled circuit can have low $g^{(2)}(0)$ in the weak coupling regime (large Γ/g) while maintaining high transmission P_{tt}. For example, a low $g^{(2)}(0) \approx 10^{-2}$ can be achieved with a $P_{tt} \approx 0.9$ for $\Gamma/g = 2$. The weak coupling condition is also beneficial as it allows the use of low-Q cavities which are readily available in many nanophotonic systems. The performance of the T circuit depends on the intercavity coupling ξ. When $\xi/g = 1$, both $g^{(2)}(0)$ and P_{tt} [Figs. 4(a) and 4(b), respectively] decrease as Γ/g decreases, similar to the inline case. In the strong coupling regime ($\Gamma/g < 1$), the T circuit significantly outperforms the inline circuit, with $g^{(2)}(0)$ at least an order of magnitude smaller and P_{tt} as much as 40% larger. The behavior of $g^{(2)}(0)$ has a qualitative change when intercavity coupling is increased to $\xi/g = 1.9$. Now, $g^{(2)}(0)$ has a dip with an extremely low minimum value $g^{(2)}(0) < 10^{-3}$ near $\Gamma/g = 1.45$. At the same time, in this weak coupling regime there is a large $P_{tt} \approx 0.85$. For the T circuit, by scanning both coupling strengths, Fig. 4(c) shows that for $\xi/g \geqslant 1$, a fanlike structure (appearing in blue color) exists wherein $g^{(2)}(0) \sim O(10^{-3})$, corresponding to strong antibunching. The valley of the fanlike structure follows the constraining relation $\Gamma/g \sim \sqrt{2.25(\xi/g - 1)}$. Figure 4(d) shows that, in general, P_{tt} increases as Γ/g increases and ξ/g decreases. For optimal antibunching, however, operation should be restricted to the valley relation, and the maximum transmission chosen within this constraint. Therefore, the optimal operating conditions are given by $\Gamma/g = 1.45$ with $\xi/g = 1.9$, at which $g^{(2)}(0) \approx 7 \times 10^{-4}$ and $P_{tt} \approx 0.85$. The curves in Fig. 4 were obtained using a particular choice of spatial width σ (which in turn means a particular choice of input bandwidth $\propto 1/\sigma$); $g^{(2)}(0)$ is numerically found to be insensitive to the particular choice of σ. Higher σ will lead to higher single- and two-photon transmission for all geometries, although the qualitative behavior will remain the same.

D. Effects of cavity and atomic dissipations

To illustrate the fundamental limitations of each configuration, we have heretofore focused on the ideal dissipationless case. Dissipation certainly is omnipresent in any cQED circuit, but specific values depend on the particular implementation. Here, we discuss in more detail the effects of dissipation under realistic experimental conditions and show that all three cQED circuits can still achieve a photon blockade in the presence

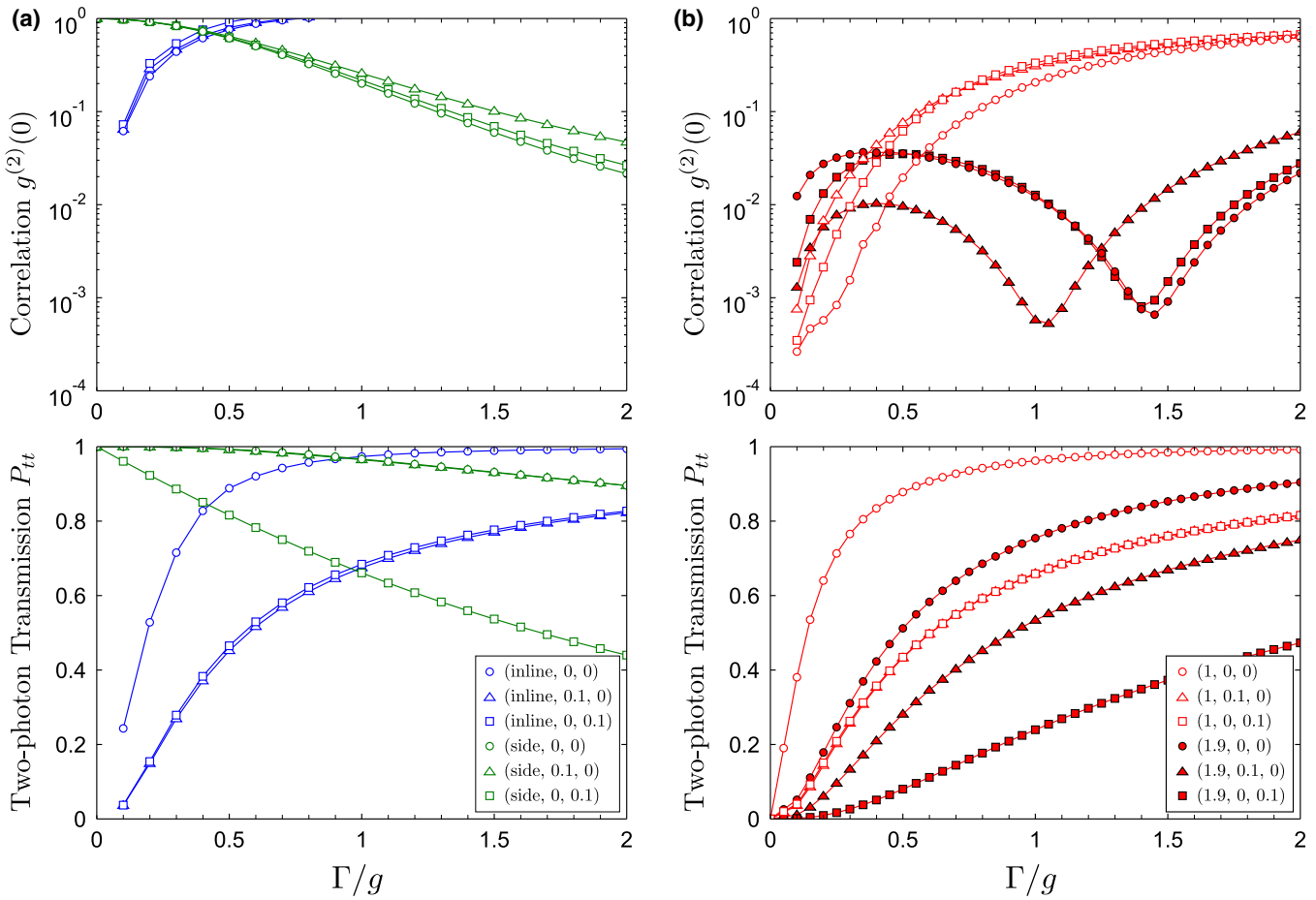

FIG. 5. (Color online) Effects of cavity and atomic dissipations. (a) Inline and side-coupled geometries. Parentheses in the legend denote (circuit type, γ_c/g, γ_a/g). (b) T geometry. Parentheses in the legend denote (ξ/g, γ_c/g, γ_a/g). Dissipation equal to $0.1g$ corresponds to or is larger than many current experimental conditions [19,21–23]).

of cavity dissipation γ_c or atomic dissipation γ_a (where the photon leaks to modes other than the privileged waveguide or cavity mode, respectively); and that the side-coupled and T cQED circuits both provide better performance compared to the inline circuit. Figure 5 plots $g^{(2)}(0)$ and P_{tt} against Γ/g with varying dissipations. For the inline circuit [the blue curves in Fig. 5(a)], $g^{(2)}(0)$ is not strongly affected by either cavity or atomic dissipation. For example, for $\Gamma/g = 0.1$ (strong coupling) and no dissipation, $g^{(2)}(0) \approx 6 \times 10^{-2}$. Cavity dissipation of $\gamma_c/g = 0.1$ does not change this value [i.e., one still has $g^{(2)}(0) \approx 6 \times 10^{-2}$], while atomic dissipation of $\gamma_a/g = 0.1$ still yields $g^{(2)}(0) \approx 7 \times 10^{-2}$. The two-photon transmission P_{tt} is, however, significantly degraded by the presence of dissipation. Cavity and atomic dissipation yield nearly identical values of P_{tt} which are significantly lower than the dissipationless case for all Γ/g. In particular, in the dissipative case, P_{tt} is 85% lower for $\Gamma/g = 0.1$.

For the side-coupled circuit [the green curves in Fig. 5(a)], cavity dissipation affects $g^{(2)}(0)$ more than atomic dissipation, but low $g^{(2)}(0) < 0.1$ can still be achieved with $\Gamma/g < 2$ for either $\gamma_c/g = 0.1$ or $\gamma_a/g = 0.1$. On the other hand, cavity dissipation has essentially no effect upon the two-photon transmission P_{tt} while atomic dissipation $\gamma_a/g = 0.1$ causes P_{tt} to fall off much more quickly with increasing Γ/g, yielding P_{tt} that is 50% lower than P_{tt} in the dissipationless case or the case with cavity dissipation only. For the T circuit with $\xi/g = 1$, $g^{(2)}(0)$ and P_{tt} still fall off monotonically as Γ/g decreases. Additionally, small $g^{(2)}(0)$ can still be achieved with either cavity or atomic dissipation. For example, one has $g^{(2)}(0) < 10^{-3}$ both $\gamma_c/g = 0.1$ and $\gamma_a/g = 0.1$. The two-photon transmission P_{tt} is reduced by an almost identical amount for either type of dissipation. For $\xi/g = 1.9$, the local minimum of $g^{(2)}(0)$ in Γ/g still appears for either cavity or atomic dissipation. In both cases, the minimum is shifted toward lower Γ/g. For the atomic case, the minimum is slightly higher than the dissipationless case, while the minimum with cavity dissipation is actually lower than the dissipationless case, meaning that an even stronger photon blockade can be achieved. The transmission is again reduced for both types of dissipation, but much less so for cavity dissipation with $P_{tt} > 0.5$ for $\Gamma/g = 1.05$ [corresponding to the minimum in $g^{(2)}(0)$ with cavity dissipation $\gamma_c/g = 0.1$], while atomic dissipation $\gamma_a/g = 0.1$ yields $P_{tt} \approx 0.35$ at $\Gamma/g = 1.4$ [corresponding to the minimum in $g^{(2)}(0)$ with atomic dissipation].

IV. SUMMARY

We have demonstrated optimal photon antibunching for two simple cQED circuits operating advantageously in the dissipatively weak coupling regime. Here, we also comment on the current experimental feasibility. To operate at the optimal conditions requires precise control of the various coupling strengths in the system. One promising implementation is in superconducting systems, wherein the coupling strength between the transmission line and the inductively coupled cavity can be adjusted over a wide range [42]. For nanophotonic systems, post-fabrication tunability is challenging, but progress has been made [43]. By operating at different single-photon frequencies [44,45], the quantum circuits can also efficiently generate extremely large bunching and super-Poissonian statistics for the transmission field. Extensions of our work include operation in modulated circuits to engineer time-dependent waveform and statistics for transmitted photons.

APPENDIX A: JAYNES-CUMMINGS AND GENERALIZED JAYNES-CUMMINGS MODELS

As stated in the main text, the Jaynes-Cummings and generalized Jaynes-Cummings models are exactly soluble from the Hamiltonian describing the coupled atom-cavity systems. In this section, we present the solutions to these models.

1. Jaynes-Cummings model

The Hamiltonian for the JC model is given by

$$H_{\rm JC} = \hbar\omega_c a_c^\dagger a_c + \hbar\omega_g a_g^\dagger a_g + \hbar\omega_e a_e^\dagger a_e + \hbar g(a_c^\dagger a_g^\dagger a_e + a_e^\dagger a_g a_c), \tag{A1}$$

where ω_c is the resonant frequency of the cavity, $\hbar\omega_g$ is the energy of the atomic ground state $|g\rangle$, and $\hbar\omega_e$ is the energy of the atomic excited state $|e\rangle$; $a_c^\dagger$ and a_c are bosonic creation and annihilation operators for photons in the cavity mode; $a_g^\dagger$ and a_g ($a_e^\dagger$ and a_e) are fermionic creation and annihilation operators for an atomic ground (excited) state.

For a given photon number n, since only the $|n,g\rangle$ and $|n-1,e\rangle$ states (where $|n,g\rangle$ and $|n,e\rangle$ correspond to n photons in the cavity and an atomic ground and excited state, respectively) are coupled by the Hamiltonian, the state can be written

$$|\psi_n\rangle = \alpha_{n,g}|n,g\rangle + \alpha_{n,e}|n-1,e\rangle, \tag{A2}$$

where $\alpha_{n,g}$ is the amplitude for n photons in cavity modes and the atom in the ground state, and $\alpha_{n,e}$ is the amplitude for $n-1$ photons in cavity modes and the atom in the excited state. Calculating the matrix elements of the Hamiltonian in this basis, one has

$$H \Rightarrow \hbar\begin{pmatrix} \omega_{\rm mid} + \left(n-\frac{1}{2}\right)\omega_c - \frac{1}{2}\Delta & \sqrt{n}g \\ \sqrt{n}g & \omega_{\rm mid} + \left(n-\frac{1}{2}\right)\omega_c + \frac{1}{2}\Delta \end{pmatrix}, \tag{A3}$$

where $\omega_{\rm mid} \equiv (\omega_e + \omega_g)/2$ is the central frequency of the atom, and $\Delta \equiv \omega_a - \omega_c$ is the detuning between the cavity resonance frequency and the atomic transition frequency $\omega_a = \omega_e - \omega_g$. From Eq. (A3), the eigenvalues are given by

$$E_n^\pm/\hbar = \omega_{\rm mid} + \left(n-\frac{1}{2}\right)\omega_c \pm \sqrt{\Delta^2/4 + ng^2}. \tag{A4}$$

These eigenvalues form the JC ladder shown schematically in Fig. 2(a) of the main text with $\Delta = 0$. The eigenstates, noted as $|n^{\pm}\rangle$, where $H|n^{\pm}\rangle = E_n^{\pm}|n^{\pm}\rangle$ are then given by

$$|n^{+}\rangle = \frac{1}{\sqrt{1+\frac{1}{4}(\bar{\Delta}+\sqrt{\bar{\Delta}^2+4})^2}}|n,g\rangle + \frac{\frac{1}{2}(\bar{\Delta}+\sqrt{\bar{\Delta}^2+4})}{\sqrt{1+\frac{1}{4}(\bar{\Delta}+\sqrt{\bar{\Delta}^2+4})^2}}|n-1,e\rangle, \tag{A5}$$

$$|n^{-}\rangle = \frac{1}{\sqrt{1+\frac{1}{4}(\bar{\Delta}-\sqrt{\bar{\Delta}^2+4})^2}}|n,g\rangle + \frac{\frac{1}{2}(\bar{\Delta}-\sqrt{\bar{\Delta}^2+4})}{\sqrt{1+\frac{1}{4}(\bar{\Delta}-\sqrt{\bar{\Delta}^2+4})^2}}|n-1,e\rangle, \tag{A6}$$

where $\bar{\Delta} \equiv \Delta/\sqrt{n}g$. For the on-resonance case (i.e., $\Delta = 0$), the amplitudes simplify to

$$|n^{+}\rangle = \frac{1}{\sqrt{2}}|n,g\rangle + \frac{1}{\sqrt{2}}|n-1,e\rangle, \tag{A7}$$

$$|n^{-}\rangle = \frac{1}{\sqrt{2}}|n,g\rangle - \frac{1}{\sqrt{2}}|n-1,e\rangle. \tag{A8}$$

The basic mechanism of the photon blockade in the inline geometry can be understood through the JC energy-level diagram [Fig. 2(a) from the main text]. Each n-photon manifold consists of two dressed states labeled $|n^{+}\rangle$ and $|n^{-}\rangle$ with a frequency separation $2\sqrt{n}g$. When a single photon at resonant frequency $\omega_i = \omega_c - g$ is injected into the inline system, it will be transmitted between waveguides with a relatively high probability as it hits a single-photon resonance $|1^{-}\rangle$ of the JC component [Fig. 2(a) bottom] and tunnels through; when two such photons are injected simultaneously, there will be a frequency mismatch of $(2-\sqrt{2})g$ with the two-photon manifold in the JC ladder, so the two photons as a whole cannot interact with the JC component and will not both be transmitted. When the JC component couples to the waveguide, the sharp energy levels will be broadened and gain a finite width Γ. For a significant frequency mismatch to occur, the inline system must therefore operate in the strong coupling regime ($g > \Gamma$).

For the side-coupled case, the injected photons have frequency $\omega_s = \omega_c$ [Fig. 2(a)]. At this operating frequency, high single-photon transmission is expected as the photon does not hit any resonance of the JC component and simply carries on unimpeded [Fig. 2(a) bottom]. When two photons are injected simultaneously, they will be antibunched and will have higher transmission efficiency than the inline case.

2. Generalized Jaynes-Cummings model

The Hamiltonian for the generalized JC model is given by

$$H_{\mathrm{GJC}} = \sum_{i=1,2} \hbar\omega_c a_{ci}^{\dagger}a_{ci} + \hbar\omega_g a_g^{\dagger}a_g + \hbar\omega_e a_e^{\dagger}a_e - \hbar\xi(a_{c2}^{\dagger}a_{c1} + a_{c1}^{\dagger}a_{c2}) + \hbar g(a_{c2}^{\dagger}a_g^{\dagger}a_e + a_e^{\dagger}a_g a_{c2}), \tag{A9}$$

where the operators $a_g^{\dagger}$ and a_g are the same as those in the previous section, and $a_{ci}^{\dagger}$ and a_{ci} are creation and annihilation operators for the ith cavity, where $i = 1$ is chosen to refer to the empty cavity and $i = 2$ to refer to the cavity containing an atom. Hereafter (and throughout the main text), it is assumed $\omega_a = \omega_c$ (i.e., the cavity and atom are on resonance). Unlike the case with the conventional JC model, the number of possible states grows with total photon number n. In particular, there will be $2n+1$ states per n-photon manifold. In the following, we compute the eigenvalues and eigenstates separately for the $n = 1$ and 2 manifolds.

a. One-photon energy levels and eigenstates

To find the energy levels of this system, we again find the matrix elements of the Hamiltonian in the appropriate basis. For $n = 1$ photon, the set of basis states is $\{|1,0,g\rangle, |0,1,g\rangle, |0,0,e\rangle\}$, where $|n_1,n_2,g\rangle = \frac{1}{\sqrt{n_1!n_2!}}(a_{c1}^{\dagger})^{n_1}(a_{c2}^{\dagger})^{n_2}a_g^{\dagger}|0\rangle$ represents a state with n_1 photons in cavity 1, n_2 photons in cavity 2, and the atom in the ground state; $|n_1,n_2,e\rangle = \frac{1}{\sqrt{n_1!n_2!}}(a_{c1}^{\dagger})^{n_1}(a_{c2}^{\dagger})^{n_2}a_e^{\dagger}|0\rangle$ corresponds to the atom in the excited state. In this basis, we find

$$H \Rightarrow \hbar\begin{pmatrix} \Omega_1 & -\xi & 0 \\ -\xi & \Omega_1 & g \\ 0 & g & \Omega_1 \end{pmatrix}, \tag{A10}$$

where $\Omega_1 \equiv \omega_g + \omega_c$. All diagonal elements are identical due to the on-resonance assumption $\omega_a = \omega_c$. The three eigenstate energies are then given by

$$E_1^0/\hbar = \Omega_1, \tag{A11}$$

$$E_1^{\pm}/\hbar = \Omega_1 \pm \sqrt{g^2+\xi^2}. \tag{A12}$$

The eigenstates can be written as

$$|1^0\rangle = \alpha_{10g}^0|1,0,g\rangle + \alpha_{01g}^0|0,1,g\rangle + \alpha_{00e}^0|0,0,e\rangle, \tag{A13}$$

$$|1^{\pm}\rangle = \alpha_{10g}^{\pm}|1,0,g\rangle + \alpha_{01g}^{\pm}|0,1,g\rangle + \alpha_{00e}^{\pm}|0,0,e\rangle, \tag{A14}$$

where $H|1^0\rangle = E_1^0|1^0\rangle$ and $H|1^{\pm}\rangle = E_1^{\pm}|1^{\pm}\rangle$. Solving for the amplitudes yields

$$\alpha_{10g}^0 = \frac{1}{\sqrt{1+\bar{\xi}^2}}, \tag{A15}$$

$$\alpha_{01g}^0 = 0, \tag{A16}$$

$$\alpha_{00e}^0 = \frac{\bar{\xi}}{\sqrt{1+\bar{\xi}^2}}, \tag{A17}$$

$$\alpha_{10g}^{+} = \frac{-\bar{\xi}}{\sqrt{2}\sqrt{1+\bar{\xi}^2}}, \tag{A18}$$

$$\alpha_{01g}^{+} = \frac{1}{\sqrt{2}}, \tag{A19}$$

$$\alpha^{+}_{00e} = \frac{1}{\sqrt{2}\sqrt{1+\bar{\xi}^2}}, \tag{A20}$$

$$\alpha^{-}_{10g} = \frac{-\bar{\xi}}{\sqrt{2}\sqrt{1+\bar{\xi}^2}}, \tag{A21}$$

$$\alpha^{-}_{01g} = -\frac{1}{\sqrt{2}}, \tag{A22}$$

$$\alpha^{-}_{00e} = \frac{1}{\sqrt{2}\sqrt{1+\bar{\xi}^2}}, \tag{A23}$$

where $\bar{\xi} \equiv \xi/g$. For the resonant case, all amplitudes are either constant or depend only on the ratio ξ/g. When $\bar{\xi}$ becomes small, the bare cavity once again decouples, and the eigenstates of the generalized JC component reduce to product states of the bare cavity state and the JC dressed state: $|\text{bare cav}\rangle \otimes |\text{JC}\rangle$. The eigenstate naming convention is chosen to make this reduction transparent: the $|1^{\pm}\rangle$ generalized JC states reduce to $|0\rangle_{\text{cav}}|1^{\pm}\rangle_{\text{JC}}$ (i.e., the photon is completely in the JC subsystem); the $|1^{0}\rangle$ generalized JC state reduces to $|1\rangle_{\text{cav}}|0\rangle_{\text{JC}}$ (i.e., the photon is in the bare cavity).

b. Two-photon energy levels and eigenstates

For $n = 2$ photons, the set of basis states becomes $\{|2,0,g\rangle, |1,1,g\rangle, |0,2,g\rangle, |1,0,e\rangle, |0,1,e\rangle\}$, where all bases are interpreted as in Sec. A 2 a. In this basis, one has

$$H \Rightarrow \hbar \begin{pmatrix} \Omega_2 & -\sqrt{2}\xi & 0 & 0 & 0 \\ -\sqrt{2}\xi & \Omega_2 & -\sqrt{2}\xi & g & 0 \\ 0 & -\sqrt{2}\xi & \Omega_2 & 0 & \sqrt{2}g \\ 0 & g & 0 & \Omega_2 & -\xi \\ 0 & 0 & \sqrt{2}g & -\xi & \Omega_2 \end{pmatrix}, \tag{A24}$$

where $\Omega_2 \equiv \omega_g + 2\omega_c$. Again, the diagonal elements are all identical due to the on-resonance assumption. The five eigenstate energies are given by

$$E^0_2/\hbar = \Omega_2, \tag{A25}$$

$$E^{-\prime}_2/\hbar = \Omega_2 - \sqrt{\frac{3g^2}{2} + \frac{5\xi^2}{2} - \frac{1}{2}\sqrt{g^4 + 30g^2\xi^2 + 9\xi^4}}, \tag{A26}$$

$$E^{+\prime}_2/\hbar = \Omega_2 + \sqrt{\frac{3g^2}{2} + \frac{5\xi^2}{2} - \frac{1}{2}\sqrt{g^4 + 30g^2\xi^2 + 9\xi^4}}, \tag{A27}$$

$$E^{-}_2/\hbar = \Omega_2 - \sqrt{\frac{3g^2}{2} + \frac{5\xi^2}{2} + \frac{1}{2}\sqrt{g^4 + 30g^2\xi^2 + 9\xi^4}}, \tag{A28}$$

$$E^{+}_2/\hbar = \Omega_2 + \sqrt{\frac{3g^2}{2} + \frac{5\xi^2}{2} + \frac{1}{2}\sqrt{g^4 + 30g^2\xi^2 + 9\xi^4}}, \tag{A29}$$

where $E^{+}_2 > E^{+\prime}_2 > E^{0}_2 > E^{-\prime}_2 > E^{-}_2$. Now, the five eigenstates are denoted $|2^+\rangle$, $|2^+\rangle'$, $|2^0\rangle$, $|2^-\rangle'$, and $|2^+\rangle$. The eigenstates are again linear combinations of the bare states. For example, the central $|2^0\rangle$ state can be written

$$|2^0\rangle = \alpha^0_{20g}|2,0,g\rangle + \alpha^0_{11g}|1,1,g\rangle + \alpha^0_{02g}|0,2,g\rangle + \alpha^0_{10e}|1,0,e\rangle + \alpha^0_{01e}|0,1,e\rangle, \tag{A30}$$

and other eigenstates can be written analogously.

Solving for the central (energy E^0_2) amplitudes yields

$$\alpha^0_{20g} = \frac{1-\bar{\xi}^2}{\sqrt{1+2\bar{\xi}^2}}, \quad \alpha^0_{11g} = 0,$$

$$\alpha^0_{02g} = \frac{\bar{\xi}^2}{\sqrt{1+2\bar{\xi}^4}}, \quad \alpha^0_{10e} = \frac{\sqrt{2}\bar{\xi}}{\sqrt{1+2\bar{\xi}^4}},$$

$$\alpha^0_{01e} = 0,$$

where $\bar{\xi} \equiv \xi/g$. The $|2^-\rangle'$ and $|2^+\rangle'$ amplitudes are given by

$$\alpha^{-\prime}_{20g} = D_1^{-1}\bar{\xi}(1 - 3\bar{\xi}^2 + R), \quad \alpha^{+\prime}_{20g} = -\alpha^{-\prime}_{20g},$$

$$\alpha^{-\prime}_{11g} = \frac{\sqrt{1 - 3\bar{\xi}^2 + R}}{2\sqrt{R}}, \quad \alpha^{+\prime}_{11g} = \alpha^{-\prime}_{11g},$$

$$\alpha^{-\prime}_{02g} = D_1^{-1}\bar{\xi}(-5 - 3\bar{\xi}^2 + R), \quad \alpha^{+\prime}_{02g} = -\alpha^{-\prime}_{02g},$$

$$\alpha^{-\prime}_{10e} = -\frac{1}{\sqrt{2}}D_1^{-1}(1 - 9\bar{\xi}^2 + R), \quad \alpha^{+\prime}_{10e} = -\alpha^{-\prime}_{10e},$$

$$\alpha^{-\prime}_{01e} = \frac{\sqrt{-1 + 3\bar{\xi}^2 + R}}{2\sqrt{R}}, \quad \alpha^{+\prime}_{01e} = \alpha^{-\prime}_{01e},$$

where

$$D_1 \equiv \sqrt{2}\sqrt{1 + R + 17\bar{\xi}^2(2-R) + 3\bar{\xi}^4(43 - 4R) + 36\bar{\xi}^6}$$

and

$$R \equiv \sqrt{1 + 30\bar{\xi}^2 + 9\bar{\xi}^4}.$$

The amplitudes corresponding to the outermost states ($|2^-\rangle$ and $|2^+\rangle$) are given by

$$\alpha^{-}_{20g} = D_2^{-1}\bar{\xi}(1 - 3\bar{\xi}^2 - R), \quad \alpha^{+}_{20g} = -\alpha^{-}_{20g},$$

$$\alpha^{-}_{11g} = \frac{-3\bar{\xi}}{\sqrt{R}\sqrt{1 - 3\bar{\xi}^2 + R}}, \quad \alpha^{+}_{11g} = \alpha^{-}_{11g},$$

$$\alpha^{-}_{02g} = -D_2^{-1}\bar{\xi}(5 + 3\bar{\xi}^2 + R), \quad \alpha^{+}_{02g} = -\alpha^{-}_{02g},$$

$$\alpha^{-}_{10e} = -\frac{1}{\sqrt{2}}D_2^{-1}(1 - 9\bar{\xi}^2 - R), \quad \alpha^{+}_{10e} = -\alpha^{-}_{10e},$$

$$\alpha^{-}_{01e} = 3D_3^{-1}\bar{\xi}, \quad \alpha^{+}_{01e} = -\alpha^{-}_{01e},$$

where

$$D_2 \equiv \sqrt{2}\sqrt{1 - R + 17\bar{\xi}^2(2+R) + 3\bar{\xi}^4(43 + 4R) + 36\bar{\xi}^6}$$

and

$$D_3 = \sqrt{1 - R + 3\bar{\xi}^2(10 + R) + 9\bar{\xi}^4}.$$

It is not immediately obvious from the expressions above, but all of the amplitudes above are real for any value of ξ. The denominator for several of the amplitudes D_2 approaches zero as $\bar{\xi}$ approaches zero, but the limit for all of the amplitudes is as $\bar{\xi} \to 0$ is finite. For the limiting case of large $\bar{\xi}$, all dressed

states are cavitylike and equally spaced in frequency. As with the $n = 1$ case, as $\bar{\xi}$ becomes small the bare cavity decouples, and the eigenstates of the generalized JC component reduce to product states of the bare cavity state and the JC dressed state: $|\text{bare cav}\rangle \otimes |\text{JC}\rangle$. The eigenstate naming convention in the $n = 2$ case is again chosen to make this reduction transparent: the $|2^{\pm}\rangle$ generalized JC states reduce to $|0\rangle_{\text{cav}}|2^{\pm}\rangle_{\text{JC}}$ (i.e., both photons are in the JC subsystem); the $|2^{\pm}\rangle'$ generalized JC states reduce to $|1\rangle_{\text{cav}}|1^{\pm}\rangle_{\text{JC}}$ (i.e., one photon is in the bare cavity, and one is in the JC subsystem); the $|2^{0}\rangle$ generalized JC state reduces to $|2\rangle_{\text{cav}}|0\rangle_{\text{JC}}$ (i.e., both photons are in the bare cavity). The T geometry operates at single-photon frequency $\omega_T = \omega_c$, so a single photon can tunnel through by interacting with the resonance $|1^{0}\rangle$ of the generalized JC system. When two photons are injected simultaneously, the two photons will hit the unperturbed resonance $|2^{0}\rangle$ of the two-photon manifold of the generalized JC component. The two photons will be antibunched with a higher transmission than the inline case.

APPENDIX B: FULL HAMILTONIAN AND EQUATIONS OF MOTION FOR EACH QUANTUM CIRCUIT

In this section, the Hamiltonian describing the full inline, side-coupled, and T geometries is shown and the respective two-photon equations of motion are derived.

1. Inline geometry

As given in Ref. [20] from the main text, the Hamiltonian for the inline geometry is

$$H = H_w + H_a + H_c + H_{wc} + H_{ac}. \tag{B1}$$

H_w is the folded Hamiltonian for photonic propagation in the two waveguide branches

$$H_w = \hbar \int dx c_l^{\dagger}(x)(-iv\partial_x)c_l(x) + \hbar \int dx c_r^{\dagger}(x)(-iv\partial_x)c_r(x), \tag{B2}$$

where the subscripts l and r refer to the left- and right-hand branches of the waveguide, respectively. The operators $c_l(x)$ and $c_l^{\dagger}(x)$ [$c_r(x)$ and $c_r^{\dagger}(x)$] are creation and annihilation operators for a photon in the left- (right-) hand branch of the waveguide. The path corresponding to each operator is shown in Fig. 6. For the left-hand branch, $c_l(x < 0)$ describes a photon moving to the right at $-|x|$ in the left-hand branch,

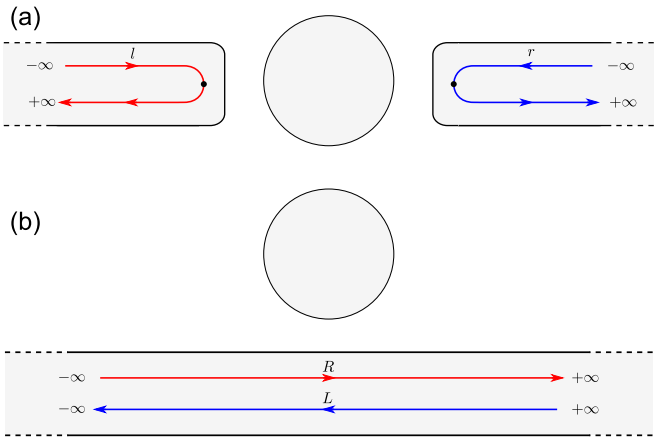

FIG. 6. (Color online) Regular and folded coordinates for describing different cavity QED geometries. (a) Folded coordinates to describe inline and T geometries, wherein photons are reflected unless they interact with the cavity. (b) Regular, left-right coordinates to describe side-coupled geometry, wherein photons continue to propagate unimpeded unless they interact with the cavity.

and $c_l(x > 0)$ describes a photon moving to the left at $-|x|$ in the left-hand branch. The operator $c_r(x)$ has a similar meaning for the right-hand branch.

$H_a + H_c + H_{ac}$ is equal to H_{JC} from the previous section. H_a is the Hamiltonian for the atom and is given by

$$H_a = \hbar\omega_g a_g^{\dagger} a_g + \hbar\omega_e a_e^{\dagger} a_e, \tag{B3}$$

where $a_g^{\dagger}$ and a_g ($a_e^{\dagger}$ and a_e) are creation and annihilation operators for the atomic ground (excited) state; $\hbar\omega_g$ and $\hbar\omega_e$ are the energies of the atomic ground state $|g\rangle$ and excited state $|e\rangle$, respectively.

H_c is the Hamiltonian for cavity modes, and is given by

$$H_c = \hbar\omega_c a_c^{\dagger} a_c, \tag{B4}$$

where $a_c^{\dagger}$ and a_c are creation and annihilation operators for cavity modes, and ω_c is the resonant frequency of the cavity.

H_{ac} describes the coupling between the atom and cavity modes, and is given by

$$H_{ac} = \hbar g(a_e^{\dagger} a_g a_c + a_c^{\dagger} a_g^{\dagger} a_e), \tag{B5}$$

where g is the atom-cavity coupling strength.

H_{wc} describes cavity-waveguide coupling to folded waveguide modes and is given by

$$H_{wc} = \int dx V_c \delta(x)[c_l^{\dagger}(x)a_c + a_c^{\dagger}c_l(x) + c_r^{\dagger}(x)a_c + a_c^{\dagger}c_r(x)], \tag{B6}$$

where V_c gives the coupling strength between waveguided and cavity modes (the cavity couples to the waveguide at $x = 0$).

The general state with only two photons present is

$$|\psi\rangle = \iint dx_1 dx_2\, \phi_{ll}(x_1,x_2,t)e^{-i\omega_g t}\frac{1}{\sqrt{2}}c_l^{\dagger}(x_1)c_l^{\dagger}(x_2)a_g^{\dagger}|0\rangle + \iint dx_1 dx_2\, \phi_{lr}(x_1,x_2,t)e^{-i\omega_g t}\frac{1}{\sqrt{2}}c_l^{\dagger}(x_1)c_r^{\dagger}(x_2)a_g^{\dagger}|0\rangle$$
$$+ \iint dx_1 dx_2\, \phi_{LR}(x_1,x_2,t)e^{-i\omega_g t}\frac{1}{\sqrt{2}}c_r^{\dagger}(x_1)c_l^{\dagger}(x_2)a_g^{\dagger}|0\rangle + \iint dx_1 dx_2\, \phi_{LL}(x_1,x_2,t)e^{-i\omega_g t}\frac{1}{\sqrt{2}}c_r^{\dagger}(x_1)c_r^{\dagger}(x_2)a_g^{\dagger}|0\rangle$$

$$+\int dx\, e_{cl}(x,t)e^{-i(\omega_g+\omega_c)t}c_l^\dagger(x)a_c^\dagger a_g^\dagger|0\rangle+\int dx\, e_{cr}(x,t)e^{-i(\omega_g+\omega_c)t}c_r^\dagger(x)a_c^\dagger a_g^\dagger|0\rangle$$
$$+\int dx\, e_{al}(x,t)e^{-i\omega_e t}c_l^\dagger(x)a_e^\dagger|0\rangle+\int dx\, e_{ar}(x,t)e^{-i\omega_e t}c_r^\dagger(x)a_e^\dagger|0\rangle+e_{cc}(t)e^{-i2\omega_c t}\frac{1}{\sqrt{2}}a_c^\dagger a_c^\dagger a_g^\dagger|0\rangle+e_{ac}(t)e^{-i(\omega_e+\omega_c)t}a_c^\dagger a_e^\dagger|0\rangle, \tag{B7}$$

where $\phi_{ll}(x_1,x_2,t)$, $\phi_{lr}(x_1,x_2,t)$, $\phi_{rl}(x_1,x_2,t)$, and $\phi_{rr}(x_1,x_2,t)$ are amplitudes corresponding to two photons in the waveguide, no cavity excitation, and the atom in the ground state; $e_{cl}(x,t)$ and $e_{cr}(x,t)$ are amplitudes corresponding to one photon in the waveguide, one cavity excitation, and the atom in the ground state; $e_{al}(x,t)$ and $e_{ar}(x,t)$ are amplitudes corresponding to one photon in the waveguide, no cavity excitation, and the atom in the excited state; $e_{cc}(t)$ is the amplitude corresponding to no photons in the waveguide, two cavity excitations, and the atom in the ground state; $e_{ac}(t)$ is the amplitude corresponding to no photons in the waveguide, one cavity excitation, and the atom in the excited state. In Eq. (B7), the phase due to the temporal evolution of the atomic and cavity parts of the state ($e^{-i\omega_g t}$, $e^{-i\omega_e t}$, and $e^{-i\omega_c}$) is written explicitly for convenience. The two-photon part of the state is symmetric under the interchange of x_1 and x_2. For the ll and rr portions, this means that $\phi_{ll}(x_1,x_2)=\phi_{ll}(x_2,x_1)$ and $\phi_{rr}(x_1,x_2)=\phi_{rr}(x_2,x_1)$. The part of the state with one photon in the left-hand branch and one in the right-hand branch is separated into lr and rl for convenience, and here symmetrization requires $\phi_{lr}(x_1,x_2)=\phi_{rl}(x_2,x_1)$.

Solving the Schrödinger equation with this Hamiltonian and state yields the equations of motion

$$\begin{aligned}
\dot\phi_{ll}(x_1,x_2,t) &= -v(\partial_{x_1}+\partial_{x_2})\phi_{ll}(x_1,x_2,t)-i\frac{V_c}{\sqrt{2}}[\delta(x_2)e_{cl}(x_1,t)+\delta(x_1)e_{cl}(x_2,t)]e^{-i\omega_c t},\\
\dot\phi_{lr}(x_1,x_2,t) &= -v(\partial_{x_1}+\partial_{x_2})\phi_{lr}(x_1,x_2,t)-i\frac{V_c}{\sqrt{2}}[\delta(x_2)e_{cl}(x_1,t)+\delta(x_1)e_{cr}(x_2,t)]e^{-i\omega_c t},\\
\dot\phi_{rl}(x_1,x_2,t) &= -v(\partial_{x_1}+\partial_{x_2})\phi_{rl}(x_1,x_2,t)-i\frac{V_c}{\sqrt{2}}[\delta(x_2)e_{cr}(x_1,t)+\delta(x_1)e_{cl}(x_2,t)]e^{-i\omega_c t},\\
\dot\phi_{rr}(x_1,x_2,t) &= -v(\partial_{x_1}+\partial_{x_2})\phi_{rr}(x_1,x_2,t)-i\frac{V_c}{\sqrt{2}}[\delta(x_2)e_{cL}(x_1,t)+\delta(x_1)e_{cL}(x_2,t)]e^{-i\omega_c t},\\
\dot e_{cl}(x,t) &= -v\partial_x e_{cl}(x,t)-i\frac{V_c}{\sqrt{2}}[\phi_{ll}(0,x,t)+\phi_{ll}(x,0,t)+\phi_{lr}(x,0,t)+\phi_{rl}(0,x,t)]e^{i\omega_c t}\\
&\quad -i\sqrt{2}V_c\delta(x)e_{cc}(t)e^{-i\omega_c t}-ige_{al}(x,t)e^{-i\Delta t},\\
\dot e_{cr}(x,t) &= -v\partial_x e_{cr}(x,t)-i\frac{V_c}{\sqrt{2}}[\phi_{rr}(0,x,t)+\phi_{rr}(x,0,t)+\phi_{lr}(0,x,t)+\phi_{rl}(x,0,t)]e^{i\omega_c t}\\
&\quad -i\sqrt{2}V_c\delta(x)e_{cc}(t)e^{-i\omega_c t}-ige_{ar}(x,t)e^{-i\Delta t},\\
\dot e_{al}(x,t) &= -v\partial_x e_{al}(x,t)-iV_c\delta(x)e_{ac}e^{-i\omega_c t}-ige_{cl}(x,t)e^{i\Delta t},\\
\dot e_{ar}(x,t) &= -v\partial_x e_{ar}(x,t)-iV_c\delta(x)e_{ac}e^{-i\omega_c t}-ige_{cr}(x,t)e^{i\Delta t},\\
\dot e_{cc}(t) &= -i\sqrt{2}V_c[e_{cl}(0,t)+e_{cr}(0,t)]e^{i\omega_c t}-i\sqrt{2}ge_{ac}(t)e^{-i\Delta t},\\
\dot e_{ac}(t) &= -iV_c[e_{al}(0,t)+e_{ar}(0,t)]e^{i\omega_c t}-i\sqrt{2}ge_{cc}(t)e^{i\Delta t}.
\end{aligned} \tag{B8}$$

The fully interacting two-photon system dynamics can be obtained by solving these equations of motion. For an arbitrary set of initial conditions, the system evolves in time according to the equations of motion to trace out the full spatiotemporal dynamics of the process.

2. Side-coupled geometry

The total Hamiltonian for the inline geometry is given by

$$H=H_w'+H_a+H_c+H_{wc}'+H_{ac}, \tag{B9}$$

where H_a, H_c, and H_{ac} are the same as those in Eq. (B1). H_w' is the photonic Hamiltonian corresponding to a single waveguide

$$H_w'=\hbar\int dx c_R^\dagger(x)(-iv\partial_x)c_R(x)+\hbar\int dx c_L^\dagger(x)(iv\partial_x)c_L(x), \tag{B10}$$

where $c_R^\dagger(x)$ and $c_R(x)$ are creation and annihilation operators for a right-moving photon at position x; $c_L^\dagger(x)$ and $c_L(x)$ are creation and annihilation operators for a left-moving photon at position x.

H_{wc}' describes cavity-waveguide coupling with regular right- and left-moving modes, and is given by

$$H_{wc}'=\int dx\, V_c\delta(x)[c_R^\dagger(x)a_c+a_c^\dagger c_R(x)+c_L^\dagger(x)a_c+a_c^\dagger c_L(x)]. \tag{B11}$$

The general state with two photons is given by

$$
\begin{aligned}
|\psi\rangle = &\iint dx_1 dx_2\, \phi_{RR}(x_1,x_2,t) e^{-i\omega_g t} \frac{1}{\sqrt{2}} c_R^\dagger(x_1) c_R^\dagger(x_2) a_g^\dagger |0\rangle + \iint dx_1 dx_2\, \phi_{RL}(x_1,x_2,t) e^{-i\omega_g t} \frac{1}{\sqrt{2}} c_R^\dagger(x_1) c_L^\dagger(x_2) a_g^\dagger |0\rangle \\
&+ \iint dx_1 dx_2\, \phi_{LR}(x_1,x_2,t) e^{-i\omega_g t} \frac{1}{\sqrt{2}} c_L^\dagger(x_1) c_R^\dagger(x_2) a_g^\dagger |0\rangle + \iint dx_1 dx_2\, \phi_{LL}(x_1,x_2,t) e^{-i\omega_g t} \frac{1}{\sqrt{2}} c_L^\dagger(x_1) c_L^\dagger(x_2) a_g^\dagger |0\rangle \\
&+ \int dx\, e_{cR}(x,t) e^{-i(\omega_g+\omega_c)t} c_R^\dagger(x) a_c^\dagger a_g^\dagger |0\rangle + \int dx\, e_{cL}(x,t) e^{-i(\omega_g+\omega_c)t} c_L^\dagger(x) a_c^\dagger a_g^\dagger |0\rangle + \int dx\, e_{aR}(x,t) e^{-i\omega_e t} c_R^\dagger(x) a_e^\dagger |0\rangle \\
&+ \int dx\, e_{aL}(x,t) e^{-i\omega_e t} c_L^\dagger(x) a_e^\dagger |0\rangle + e_{cc}(t) e^{-i2\omega_c t} \frac{1}{\sqrt{2}} a_c^\dagger a_c^\dagger a_g^\dagger |0\rangle + e_{ac}(t) e^{-i(\omega_e+\omega_c)t} a_c^\dagger a_e^\dagger |0\rangle, \qquad \text{(B12)}
\end{aligned}
$$

where the amplitudes have analogous meanings to those for the inline cavity, except that RR, LL, RL, and LR terms indicate the direction of travel for the photons rather than which branch of the waveguide they are in.

Solving the Schrödinger equation with this Hamiltonian and state yields the equations of motion

$$
\begin{aligned}
\dot{\phi}_{RR}(x_1,x_2,t) &= -v\left(\partial_{x_1} + \partial_{x_2}\right)\phi_{RR}(x_1,x_2,t) - i\frac{V_c}{\sqrt{2}}[\delta(x_2) e_{cR}(x_1,t) + \delta(x_1) e_{cR}(x_2,t)] e^{-i\omega_c t}, \\
\dot{\phi}_{RL}(x_1,x_2,t) &= \left(-v\partial_{x_1} + v\partial_{x_2}\right)\phi_{RL}(x_1,x_2,t) - i\frac{V_c}{\sqrt{2}}[\delta(x_2) e_{cR}(x_1,t)\delta(x_1) e_{cL}(x_2,t)] e^{-i\omega_c t}, \\
\dot{\phi}_{LR}(x_1,x_2,t) &= \left(v\partial_{x_1} - v\partial_{x_2}\right)\phi_{LR}(x_1,x_2,t) - i\frac{V_c}{\sqrt{2}}[\delta(x_2) e_{cL}(x_1,t) + \delta(x_1) e_{cR}(x_2,t)] e^{-i\omega_c t}, \\
\dot{\phi}_{LL}(x_1,x_2,t) &= v\left(\partial_{x_1} + \partial_{x_2}\right)\phi_{LL}(x_1,x_2,t) - i\frac{V_c}{\sqrt{2}}[\delta(x_2) e_{cL}(x_1,t) + \delta(x_1) e_{cL}(x_2,t)] e^{-i\omega_c t}, \\
\dot{e}_{cR}(x,t) &= -v\partial_x e_{cR}(x,t) - i\frac{V_c}{\sqrt{2}}[\phi_{RR}(0,x,t) + \phi_{RR}(x,0,t) + \phi_{RL}(x,0,t) + \phi_{LR}(0,x,t)] e^{i\omega_c t} \\
&\quad - i\sqrt{2} V_c \delta(x) e_{cc}(t) e^{-i\omega_c t} - i g e_{aR}(x,t) e^{-i\Delta t}, \\
\dot{e}_{cL}(x,t) &= v\partial_x e_{cL}(x,t) - i\frac{V_c}{\sqrt{2}}[\phi_{LL}(0,x,t) + \phi_{LL}(x,0,t) + \phi_{RL}(0,x,t) - i\phi_{LR}(x,0,t)] e^{i\omega_c t} \\
&\quad - i\sqrt{2} V_c \delta(x) e_{cc}(t) e^{-i\omega_c t} - i g e_{aL}(x,t) e^{-i\Delta t}, \\
\dot{e}_{aR}(x,t) &= -v\partial_x e_{aR}(x,t) - i V_c \delta(x) e_{ac} e^{-i\omega_c t} - i g e_{cR}(x,t) e^{i\Delta t}, \\
\dot{e}_{aL}(x,t) &= v\partial_x e_{aL}(x,t) - i V_c \delta(x) e_{ac} e^{-i\omega_c t} - i g e_{cL}(x,t) e^{i\Delta t}, \\
\dot{e}_{cc}(t) &= -i\sqrt{2} V_c [e_{cR}(0,t) + e_{cL}(0,t)] e^{i\omega_c t} - i\sqrt{2} g e_{ac}(t) e^{-i\Delta t}, \\
\dot{e}_{ac}(t) &= -i V_c [e_{aR}(0,t) + e_{aL}(0,t)] e^{i\omega_c t} - i\sqrt{2} g e_{cc}(t) e^{i\Delta t}. \qquad \text{(B13)}
\end{aligned}
$$

As for the inline geometry, the fully interacting two-photon dynamics can be obtained by solving these equations of motion. This set of equations is largely similar to those describing the inline system, but with left- and right-moving modes rather than two folded chiral modes.

3. T geometry

The total Hamiltonian for the T geometry is given by

$$H = H_w + H_a + H_c' + H_{wc}'' + H_{cc} + H_{ac}', \qquad \text{(B14)}$$

where H_w is the folded photonic Hamiltonian given in Eq. (B2), and H_a is the same as that given previously. Other terms are similar to those for the inline case, but with multiple cavities. H_c' is given by a sum over terms equivalent to the previous cavity Hamiltonian

$$H_c' = \sum_{i=1,2} \hbar\omega_c a_{ci}^\dagger a_{ci}, \qquad \text{(B15)}$$

where $a_{ci}^\dagger$ and a_{ci} are creation and annihilation operators for the ith cavity, where $i = 1$ refers to the bare cavity and $i = 2$ refers to the cavity containing an atom.

H_{wc}'' is analogous to H_{wc}', but with the necessary subscripts to indicate that the folded waveguide modes couple to cavity 1:

$$
\begin{aligned}
H_{wc}'' = \int dx\, V_c \delta(x) [&c_l^\dagger(x) a_{c1} + a_{c1}^\dagger c_l(x) + c_r^\dagger(x) a_{c1} \\
&+ a_{c1}^\dagger c_r(x)]. \qquad \text{(B16)}
\end{aligned}
$$

H_{cc} describes cavity-cavity coupling and is given by

$$H_{cc} = -\hbar\xi(a_{c2}^\dagger a_{c1} + a_{c1}^\dagger a_{c2}), \qquad \text{(B17)}$$

where the sign can be determined by a symmetry argument.

H'_{ac} is equivalent to H_{ac} but with a subscript to indicate that the atom couples to cavity 2:

$$H'_{ac} = \hbar g(a^\dagger_{c2}a^\dagger_g a_e + a^\dagger_e a_g a_{c2}). \tag{B18}$$

The part of the Hamiltonian $H_a + H'_c + H_{cc} + H'_{ac}$ is equal to the generalized JC Hamiltonian H_{GJC} from the previous section.

The general two-photon state for the T geometry is given by

$$\begin{aligned}
|\psi\rangle = &\iint dx_1 dx_2\, \phi_{ll}(x_1,x_2,t)e^{-i\omega_g t}\frac{1}{\sqrt{2}}c^\dagger_l(x_1)c^\dagger_l(x_2)a^\dagger_g|0\rangle + \iint dx_1 dx_2\, \phi_{lr}(x_1,x_2,t)e^{-i\omega_g t}\frac{1}{\sqrt{2}}c^\dagger_l(x_1)c^\dagger_r(x_2)a^\dagger_g|0\rangle \\
&+ \iint dx_1 dx_2\, \phi_{LR}(x_1,x_2,t)e^{-i\omega_g t}\frac{1}{\sqrt{2}}c^\dagger_r(x_1)c^\dagger_l(x_2)a^\dagger_g|0\rangle + \iint dx_1 dx_2\, \phi_{LL}(x_1,x_2,t)e^{-i\omega_g t}\frac{1}{\sqrt{2}}c^\dagger_r(x_1)c^\dagger_r(x_2)a^\dagger_g|0\rangle \\
&+ \int dx\, e_{c1l}(x,t)e^{-i(\omega_g+\omega_c)t}c^\dagger_l(x)a^\dagger_{c1}a^\dagger_g|0\rangle + \int dx\, e_{c1r}(x,t)e^{-i(\omega_g+\omega_c)t}c^\dagger_r(x)a^\dagger_{c1}a^\dagger_g|0\rangle \\
&+ \int dx\, e_{c2l}(x,t)e^{-i(\omega_g+\omega_c)t}c^\dagger_l(x)a^\dagger_{c2}a^\dagger_g|0\rangle + \int dx\, e_{c2r}(x,t)e^{-i(\omega_g+\omega_c)t}c^\dagger_r(x)a^\dagger_{c2}a^\dagger_g|0\rangle + \int dx\, e_{al}(x,t)e^{-i\omega_e t}c^\dagger_l(x)a^\dagger_e|0\rangle \\
&+ \int dx\, e_{ar}(x,t)e^{-i\omega_e t}c^\dagger_r(x)a^\dagger_e|0\rangle + e_{c1c1}(t)e^{-i2\omega_c t}\frac{1}{\sqrt{2}}a^\dagger_{c1}a^\dagger_{c1}a^\dagger_g|0\rangle + e_{c1c2}(t)e^{-i2\omega_c t}a^\dagger_{c1}a^\dagger_{c2}a^\dagger_g|0\rangle \\
&+ e_{c2c2}(t)e^{-i2\omega_c t}\frac{1}{\sqrt{2}}a^\dagger_{c2}a^\dagger_{c2}a^\dagger_g|0\rangle + e_{c1a}(t)e^{-i(\omega_e+\omega_c)t}a^\dagger_{c1}a^\dagger_e|0\rangle + e_{c2a}(t)e^{-i(\omega_e+\omega_c)t}a^\dagger_{c2}a^\dagger_e|0\rangle,
\end{aligned} \tag{B19}$$

where all terms have analogous meanings to those described for the inline geometry.

Solving the Schrödinger equation with this Hamiltonian and state yields the equations of motion

$$\begin{aligned}
\dot\phi_{ll}(x_1,x_2,t) &= -v\big(\partial_{x_1}+\partial_{x_2}\big)\phi_{ll}(x_1,x_2,t) - i\frac{V_c}{\sqrt{2}}[\delta(x_2)e_{cl}(x_1,t)+\delta(x_1)e_{cl}(x_2,t)]e^{-i\omega_c t}, \\
\dot\phi_{lr}(x_1,x_2,t) &= -v\big(\partial_{x_1}+\partial_{x_2}\big)\phi_{lr}(x_1,x_2,t) - i\frac{V_c}{\sqrt{2}}[\delta(x_2)e_{cl}(x_1,t)+\delta(x_1)e_{cr}(x_2,t)]e^{-i\omega_c t}, \\
\dot\phi_{rl}(x_1,x_2,t) &= -v\big(\partial_{x_1}+\partial_{x_2}\big)\phi_{rl}(x_1,x_2,t) - i\frac{V_c}{\sqrt{2}}[\delta(x_2)e_{cr}(x_1,t)+\delta(x_1)e_{cl}(x_2,t)]e^{-i\omega_c t}, \\
\dot\phi_{rr}(x_1,x_2,t) &= -v\big(\partial_{x_1}+\partial_{x_2}\big)\phi_{rr}(x_1,x_2,t) - i\frac{V_c}{\sqrt{2}}[\delta(x_2)e_{cL}(x_1,t)+\delta(x_1)e_{cL}(x_2,t)]e^{-i\omega_c t}, \\
\dot e_{c1l}(x,t) &= -v\partial_x e_{c1l}(x,t) - i\frac{V_c}{\sqrt{2}}[\phi_{ll}(0,x,t)+\phi_{ll}(x,0,t)+\phi_{lr}(x,0,t)+\phi_{rl}(0,x,t)]e^{i\omega_c t} \\
&\quad + i\xi e_{c2l}(x,t) - i\sqrt{2}V_c\delta(x)e_{c1c1}(t)e^{-i\omega_c t}, \\
\dot e_{c1r}(x,t) &= -v\partial_x e_{c1r}(x,t) - i\frac{V_c}{\sqrt{2}}[\phi_{rr}(0,x,t)+\phi_{rr}(x,0,t)+\phi_{lr}(0,x,t)+\phi_{rl}(x,0,t)]e^{i\omega_c t} \\
&\quad + i\xi e_{c2r}(x,t) - i\sqrt{2}V_c\delta(x)e_{c1c1}(t)e^{-i\omega_c t}, \\
\dot e_{c2l}(x,t) &= -v\partial_x e_{c2l}(x,t) + i\xi e_{c1l}(x,t) - ige_{al}(x,t)e^{-i\Delta t} - iV\delta(x)e_{c1c2}(t)e^{-i\omega_c t}, \\
\dot e_{c2r}(x,t) &= -v\partial_x e_{c2r}(x,t) + i\xi e_{c1r}(x,t) - ige_{ar}(x,t)e^{-i\Delta t} - iV\delta(x)e_{c1c2}(t)e^{-i\omega_c t}, \\
\dot e_{al}(x,t) &= -v\partial_x e_{al}(x,t) - iV_c\delta(x)e_{ac}e^{-i\omega_c t} - ige_{c2l}(x,t)e^{i\Delta t}, \\
\dot e_{ar}(x,t) &= -v\partial_x e_{ar}(x,t) - iV_c\delta(x)e_{ac}e^{-i\omega_c t} - ige_{c2r}(x,t)e^{i\Delta t}, \\
\dot e_{c1c1}(t) &= -i\sqrt{2}V_c[e_{c1l}(0,t)+e_{c1r}(0,t)]e^{i\omega_c t} + i\sqrt{2}\xi e_{c1c2}(t), \\
\dot e_{c1c2}(t) &= -iV_c[e_{c2l}(0,t)+e_{c2r}(0,t)]e^{i\omega_c t} + i\sqrt{2}\xi e_{c1c1}(t) + i\sqrt{2}\xi e_{c2c2}(t) - ige_{c1a}(t)e^{-i\Delta t}, \\
\dot e_{c2c2}(t) &= +i\sqrt{2}\xi e_{c1c2}(t) - i\sqrt{2}ge_{c2a}(t)e^{-i\Delta t}, \\
\dot e_{c1a}(t) &= -iV_c[e_{al}(0,t) - ie_{ar}(0,t)]e^{i\omega_c t} - ige_{c1c2}(t)e^{i\Delta t} + i\xi e_{c2a}(t), \\
\dot e_{c2a}(t) &= -i\sqrt{2}ge_{c2c2}(t)e^{i\Delta t} + i\xi e_{c1a}(t).
\end{aligned} \tag{B20}$$

Again, the full two-photon system dynamics can be obtained by solving these equations of motion.

APPENDIX C: SIMULATION OF A WEAK COHERENT STATE

As mentioned in the main text, to properly simulate a weak coherent input, one should use a truncated coherent input that contains the vacuum state, a one-photon state, and a two-photon state. A coherent state $|\alpha\rangle$ with expected photon number $\bar{n} = |\alpha|^2$ is written

$$|\alpha\rangle = \sum_{n=0}^{\infty} c_n |n\rangle, \tag{C1}$$

where

$$c_n = e^{-\bar{n}/2} \frac{\alpha^n}{\sqrt{n!}} \tag{C2}$$

and $|n\rangle$ is a photon number (Fock) state. With the real-space representation used in this work, such a number state is written

$$|n\rangle = \frac{1}{\sqrt{n!}} \left[\prod_{i=1}^{n} \int dx_i \, \phi(x_i) c_R^\dagger(x_i) \right] |0\rangle, \tag{C3}$$

that is, the photons are independent and completely spatially overlapping with spatial distribution given by $\phi(x)$ which has normalization $\int dx \, |\phi(x)|^2 = 1$. Equation (C3) supposes a right-moving coherent state. A left-moving coherent state would be generated by replacing the right-moving photonic creation operator.

The second-order correlation function (considering right-moving modes) is given by

$$g^{(2)}(\tau) = \frac{\langle c_R^\dagger(x_m) c_R^\dagger(x_m + v\tau) c_R(x_m + v\tau) c_R(x_m) \rangle}{\langle c_R^\dagger(x_m) c_R(x_m) \rangle \, \langle c_R^\dagger(x_m + v\tau) c_R(x_m + v\tau) \rangle}, \tag{C4}$$

where x_o is a reference location. Analytically, the resulting second-order correlation should not depend upon the choice of x_m, but we find that choosing x_m to correspond to the center of the pulse (either scattered or input) yields better numerical accuracy. Calculating the second-order correlation for a coherent state described by Eq. (C1), one finds $g^{(2)}(\tau) = 1$ for all τ as expected.

For a weak coherent state, the amplitudes c_n will be vanishingly small for $n > 2$, so the state can be approximated by

$$|\alpha\rangle' = c_0'|0\rangle + c_1'|1\rangle + c_2'|2\rangle, \tag{C5}$$

where the amplitudes c_n' are the same as the full coherent state amplitudes c_n but normalized such that $|c_0'|^2 + |c_1'|^2 + |c_2'|^2 = 1$. With such a state, one still finds $g^{(2)}(\tau) = 1$ for all τ. Such a truncated coherent state therefore faithfully represents an input weak coherent state. After choosing the input state corresponding to the two-photon pulse given in the main text, we then find the scattered second-order correlation by evolving the state until all cavity and atomic excitations have died down and calculating $g^{(2)}(\tau)$ for the transmitted part of the state. Note that the zero- and one-photon parts of the state only affect the normalization (not the shape) of $g^{(2)}(\tau)$, so the second-order correlation function can also be calculated by considering only the two-photon part of the scattering process and multiplying by 2 [since for a two-photon input Fock state one has $g^{(2)}(\tau) = \frac{1}{2}$ for all τ].

[1] R. J. Glauber, The quantum theory of optical coherence, Phys. Rev. **130**, 2529 (1963).

[2] L. Mandel and E. Wolf, *Optical Coherence and Quantum Optics* (Cambridge University Press, Cambridge, UK, 1995).

[3] M. O. Scully and M. S. Zubairy, *Quantum Optics* (Cambridge University Press, Cambridge, UK, 1997).

[4] R. J. Glauber, *Quantum Theory of Optical Coherence: Selected Papers and Lectures* (Wiley, Weinheim, 2007).

[5] D. F. Walls and G. J. Milburn, *Quantum Optics*, 2nd ed. (Springer, New York, 2008).

[6] S. Singh, Antibunching, sub-poissonian photon statistics and finite bandwidth effects in resonance fluorescence, Opt. Commun. **44**, 254 (1983).

[7] X. T. Zou and L. Mandel, Photon-antibunching and sub-poissonian photon statistics, Phys. Rev. A **41**, 475 (1990).

[8] P. Michler *et al.*, A quantum dot single-photon turnstile device, Science **290**, 2282 (2000).

[9] C. Kurtsiefer, S. Mayer, P. Zarda, and H. Weinfurter, Stable solid-state source of single photons, Phys. Rev. Lett. **85**, 290 (2000).

[10] A. Houck *et al.*, Generating single microwave photons in a circuit, Nature (London) **449**, 328 (2007).

[11] C. H. Bennett and G. Brassard, Quantum cryptography: Public key distribution and coin tossing, in *Proceedings of IEEE International Conference on Computers, Systems and Signal Processing* (IEEE, New York, 1984), p. 175.

[12] P. Grangier, G. Roger, and A. Aspect, Experimental evidence for a photon anticorrelation effect on a beam splitter: A new light on single-photon interferences, Europhys. Lett. **1**, 173 (1986).

[13] P. Kwiat, H. Weinfurter, T. Herzog, A. Zeilinger, and M. A. Kasevich, Interaction-free measurement, Phys. Rev. Lett. **74**, 4763 (1995).

[14] E. Knill, R. Laflamme, and G. J. Milburn, A scheme for efficient quantum computation with linear optics, Nature (London) **409**, 46 (2001).

[15] H. Carmichael and D. Walls, Proposal for the measurement of the resonant Stark effect by photon correlation techniques, J. Phys. B: At. Mol. Phys. **9**, L43 (1976).

[16] H. Kimble and L. Mandel, Theory of resonance fluorescence, Phys. Rev. A **13**, 2123 (1976).

[17] H. J. Kimble, M. Dagenais, and L. Mandel, Photon antibunching in resonance fluorescence, Phys. Rev. Lett. **39**, 691 (1977).

[18] J. T. Hoffges, H. W. Baldauf, T. Eichler, S. R. Helmfrid, and H. Walther, Heterodyne measurement of the fluorescent radiation of a single trapped ion, Opt. Commun. **133**, 170 (1997).

[19] K. M. Birnbaum *et al.*, Photon blockade in an optical cavity with one trapped atom, Nature (London) **436**, 87 (2005).

[20] K. Hennessy *et al.*, Quantum nature of a strongly coupled single quantum dot-cavity system, Nature (London) **445**, 896 (2007).
[21] A. Faraon *et al.*, Coherent generation of non-classical light on a chip via photon-induced tunneling and blockade, Nat. Phys **4**, 859 (2008).
[22] C. Lang *et al.*, Observation of resonant photon blockade at microwave frequencies using correlation function measurements, Phys. Rev. Lett. **106**, 243601 (2011).
[23] A. Reinhard *et al.*, Strongly correlated photons on a chip, Nat. Photon. **6**, 93 (2012).
[24] D. Press, S. Gotzinger, S. Reitzenstein, C. Hofmann, A. Loffler, M. Kamp, A. Forchel, and Y. Yamamoto, Photon antibunching from a single quantum-dot-microcavity system in the strong coupling regime, Phys. Rev. Lett. **98**, 117402 (2007).
[25] A. Muller, E. B. Flagg, P. Bianucci, X. Y. Wang, D. G. Deppe, W. Ma, J. Zhang, G. J. Salamo, M. Xiao, and C. K. Shih, Resonance fluorescence from a coherently driven semiconductor quantum dot in a cavity, Phys. Rev. Lett. **99**, 187402 (2007).
[26] D. Englund *et al.*, Deterministic coupling of a single nitrogen vacancy center to a photonic crystal cavity, Nano Lett. **10**, 3922 (2010).
[27] S. Rebić, A. S. Parkins, and S. M. Tan, Photon statistics of a single-atom intracavity system involving electromagnetically induced transparency, Phys. Rev. A **65**, 063804 (2002).
[28] P. Barberis-Blostein, D. G. Norris, L. A. Orozco, and H. J. Carmichael, From quantum feedback to probabilistic error correction: manipulation of quantum beats in cavity qed, New J. Phys. **12**, 023002 (2010).
[29] M. Koch, C. Sames, M. Balbach, H. Chibani, A. Kubanek, K. Murr, T. Wilk, and G. Rempe, Three-photon correlations in a strongly driven atom-cavity system, Phys. Rev. Lett. **107**, 023601 (2011).
[30] J. A. Souza, E. Figueroa, H. Chibani, C. J. Villas-Boas, and G. Rempe, Coherent control of quantum fluctuations using cavity electromagnetically induced transparency, Phys. Rev. Lett. **111**, 113602 (2013).
[31] M. Bajcsy, A. Majumdar, A. Rundquist, and J. Vučković, Photon blockade with a four-level quantum emitter coupled to a photonic-crystal nanocavity, New J. Phys. **15**, 025014 (2013).
[32] A. L. Grimsmo and S. Parkins, Open rabi model with ultrastrong coupling plus large dispersive-type nonlinearity: Nonclassical light via a tailored degeneracy, Phys. Rev. A **89**, 033802 (2014).
[33] A. V. Gorshkov, J. Otterbach, M. Fleischhauer, T. Pohl, and M. D. Lukin, Photon-photon interactions via rydberg blockade, Phys. Rev. Lett. **107**, 133602 (2011).
[34] T. Peyronel *et al.*, Quantum nonlinear optics with single photons enabled by strongly interacting atoms, Nature (London) **488**, 57 (2012).
[35] B. Dayan *et al.*, A photon turnstile dynamically regulated by one atom, Science **319**, 1062 (2008).
[36] T. Aoki, A. S. Parkins, D. J. Alton, C. A. Regal, B. Dayan, E. Ostby, K. J. Vahala, and H. J. Kimble, Efficient routing of single photons by one atom and a microtoroidal cavity, Phys. Rev. Lett. **102**, 083601 (2009).
[37] E. T. Jaynes and F. W. Cummings, Comparison of quantum and semiclassical radiation theories with application to the beam maser, Proc. IEEE **51**, 89 (1963).
[38] B. W. Shore and P. L. Knight, The Jaynes-Cummings model, J. Mod. Opt. **40**, 1195 (1993).
[39] K. K. Y. Lee, Y. Avniel, and S. G. Johnson, Design strategies and rigorous conditions for single-polarization single-mode waveguides, Opt. Express **16**, 15170 (2008).
[40] L. Tian and H. J. Carmichael, Quantum trajectory simulations of two-state behavior in an optical cavity containing one atom, Phys. Rev. A **46**, R6801(R) (1992).
[41] J.-T. Shen and S. Fan, Theory of single-photon transport in a single-mode waveguide. I. coupling to a cavity containing a two-level atom, Phys. Rev. A **79**, 023837 (2009).
[42] Y. Yin *et al.*, Catch and release of microwave photon states, Phys. Rev. Lett. **110**, 107001 (2013).
[43] D. Englund *et al.*, Controlling cavity reflectivity with a single quantum dot, Nature (London) **450**, 857 (2007).
[44] R. J. Brecha, P. R. Rice, and M. Xiao, N two-level atoms in a driven optical cavity: Quantum dynamics of forward photon scattering for weak incident fields, Phys. Rev. A **59**, 2392 (1999).
[45] H. Carmichael, R. Brecha, and P. Rice, Quantum interference and collapse of the wave function in cavity QED, Opt. Commun. **82**, 73 (1991).